doi:10.1093/brain/awy120 BRAIN 2018: 141; 2112–2126 | 2112

BRAIN
A JOURNAL OF NEUROLOGY

A lexical semantic hub for heteromodal naming in middle fusiform gyrus

Kiefer James Forseth,[1] Cihan Mehmet Kadipasaoglu,[1] Christopher Richard Conner,[1] Gregory Hickok,[2] Robert Thomas Knight[3] and Nitin Tandon[1,4]

Semantic memory underpins our understanding of objects, people, places, and ideas. Anomia, a disruption of semantic memory access, is the most common residual language disturbance and is seen in dementia and following injury to temporal cortex. While such anomia has been well characterized by lesion symptom mapping studies, its pathophysiology is not well understood. We hypothesize that inputs to the semantic memory system engage a specific heteromodal network hub that integrates lexical retrieval with the appropriate semantic content. Such a network hub has been proposed by others, but has thus far eluded precise spatiotemporal delineation. This limitation in our understanding of semantic memory has impeded progress in the treatment of anomia. We evaluated the cortical structure and dynamics of the lexical semantic network in driving speech production in a large cohort of patients with epilepsy using electrocorticography ($n = 64$), functional MRI ($n = 36$), and direct cortical stimulation ($n = 30$) during two generative language processes that rely on semantic knowledge: visual picture naming and auditory naming to definition. Each task also featured a non-semantic control condition: scrambled pictures and reversed speech, respectively. These large-scale data of the left, language-dominant hemisphere uniquely enable convergent, high-resolution analyses of neural mechanisms characterized by rapid, transient dynamics with strong interactions between distributed cortical substrates. We observed three stages of activity during both visual picture naming and auditory naming to definition that were serially organized: sensory processing, lexical semantic processing, and articulation. Critically, the second stage was absent in both the visual and auditory control conditions. Group activity maps from both electrocorticography and functional MRI identified heteromodal responses in middle fusiform gyrus, intraparietal sulcus, and inferior frontal gyrus; furthermore, the spectrotemporal profiles of these three regions revealed coincident activity preceding articulation. Only in the middle fusiform gyrus did direct cortical stimulation disrupt both naming tasks while still preserving the ability to repeat sentences. These convergent data strongly support a model in which a distinct neuroanatomical substrate in middle fusiform gyrus provides access to object semantic information. This under-appreciated locus of semantic processing is at risk in resections for temporal lobe epilepsy as well as in trauma and strokes that affect the inferior temporal cortex—it may explain the range of anomic states seen in these conditions. Further characterization of brain network behaviour engaging this region in both healthy and diseased states will expand our understanding of semantic memory and further development of therapies directed at anomia.

1 Vivian L Smith Department of Neurosurgery, McGovern Medical School, Houston, TX, USA
2 Department of Cognitive Sciences, University of California, Irvine, CA, USA
3 Department of Psychology, University of California, Berkeley, CA, USA
4 Memorial Hermann Hospital, Texas Medical Center, Houston, TX, USA

Correspondence to: Nitin Tandon
Professor, Department of Neurosurgery
UT Health Science Center
6431 Fannin Street G550D
Houston, TX 77030 USA
E-mail: nitin.tandon@uth.tmc.edu

Received January 23, 2018. Revised March 3, 2018. Accepted March 23, 2018. Advance Access publication May 30, 2018

Keywords: intracranial EEG; aphasia; temporal lobe; gamma oscillations; language

Abbreviations: BGA = broadband gamma activity; BOLD = blood oxygen level-dependent; ECoG = electrocorticography; IFG = inferior frontal gyrus; pMTG = posterior middle temporal gyrus; SB-MEMA = surface-based mixed-effects multilevel analysis; SMA = supplementary motor area

Introduction

Semantic memory is the understanding of objects, people, places, and ideas independent of reference to a specific instance (Quillian, 1966; Tulving, 1972). This repository of conceptual associations is accessible by multiple lead-in processes that, when used in the service of language, drive lexical retrieval to enable speech production (Indefrey and Levelt, 2004). Semantic memory enables us to fluently name aloud an object that we see or hear described; yet it is easily disrupted, resulting in 'tip of the tongue' phenomena in healthy individuals (Brown and McNeill, 1966) and pervasive anomias following a variety of brain injuries (Margolin *et al.*, 1990).

Prior studies of semantic memory have been largely mediated by analysis of disease (Warrington, 1975; Nestor *et al.*, 2006; Binney *et al.*, 2010; Mion *et al.*, 2010), functional imaging (Damasio *et al.*, 1996; Noppeney and Price, 2002; Bright *et al.*, 2004; Sharp *et al.*, 2004; Spitsyna *et al.*, 2006; Binder *et al.*, 2009), and non-invasive electrophysiology (Marinkovic *et al.*, 2003). These tools have yielded many insights into the complex network underlying conceptual access; however, they are limited by inherent constraints on their spatiotemporal resolution. Vascular lesions caused by middle cerebral artery strokes largely affect perisylvian cortex (Phan *et al.*, 2009), while regions within watershed zones (e.g. ventral temporal cortex) are typically only impaired by global cerebral ischaemic effects. Degenerative conditions like semantic dementia affect a diffuse set of cortical structures, challenging the precise localization of neural processes (Mion *et al.*, 2010). Experiments in healthy subjects are confronted by anatomical limitations as well: mastoid air cells result in susceptibility artefacts that degrade echo-planar imaging of ventral temporal cortex (Ojemann *et al.*, 1997; Devlin *et al.*, 2000), repetitive transcranial magnetic stimulation is unable to access the ventral pial surface (Binney *et al.*, 2010), and magnetoencephalography is relatively insensitive to magnetic fields oriented tangentially to the detectors (Hansen *et al.*, 2010).

Direct electrocorticography (ECoG) with implanted intracranial electrodes yields millimetre spatial and millisecond temporal resolution of cortical activity. Broadband gamma activity (BGA, 60–120 Hz) in these ECoG recordings is especially relevant to the study of cognition (Crone *et al.*, 2001; Jacobs and Kahana, 2010; Lachaux *et al.*, 2012). This activity arises from the focal summation of postsynaptic currents coupled with a surge in spike rate (Manning *et al.*, 2009; Lachaux *et al.*, 2012), indexing local processing (Logothetis, 2003; Cardin *et al.*, 2009; Magri *et al.*, 2012). BGA correlates strongly with the functional MRI blood oxygen level-dependent (BOLD) signal and, with its superior temporal resolution, can precisely characterize interregional timing (Mukamel *et al.*, 2005; Conner *et al.*, 2011). Additionally, intracranial electrodes allow for direct electrical stimulation that transiently mimics focal lesions, enabling study of both normal functional activation and multiple lesions in each patient (Nakai *et al.*, 2017).

In the context of speech production tasks, we hypothesize that various input modalities feeding into the semantic memory system drive a pre-phonological network hub to achieve lexical retrieval from semantic content. This hub should act as a convergence zone for networks supporting word production. A precise spatiotemporal delineation of cortical regions recruited for heteromodal (visual and auditory) naming tasks will isolate this lexical semantic convergence hub.

We used ECoG recordings in a large cohort ($n = 64$) of patients undergoing localization of epileptic foci with either surface grid or depth probe electrodes to categorize cortical responses during cued naming tasks using visual or auditory inputs: picture naming and naming to description. Each experiment was paired with a modality-specific non-semantic control: scrambled images and reversed speech. A subset of patients also underwent functional MRI prior to surgery ($n = 36$) and/or direct cortical stimulation after electrode implantation ($n = 30$). First, a surface-based mixed-effects multilevel analysis was used to yield a precise cortical effect estimate of BGA and BOLD signals across the population with ECoG and functional MRI data, respectively. Second, these activity maps were used to direct a region of interest analysis that evaluated the timing, magnitude, and spectral profile of the distributed cortical response. Third, naming disruption caused by direct cortical stimulation was integrated across the cohort.

Materials and methods

Population

Sixty-four patients with intractable epilepsy scheduled for intracranial electrode implants to localize seizure onset sites were enrolled in the study after obtaining informed consent; these patients performed cued naming tasks during ECoG. Of this cohort, 36 patients were enrolled in a preoperative language functional MRI study and 30 underwent direct cortical stimulation for the localization of eloquent cortex. Study design was approved by the University of Texas Health Science Center's committee for the protection of human subjects.

Left-hemispheric language dominance was confirmed in all 64 patients (25 males, 39 females; mean age 33 ± 10 years,

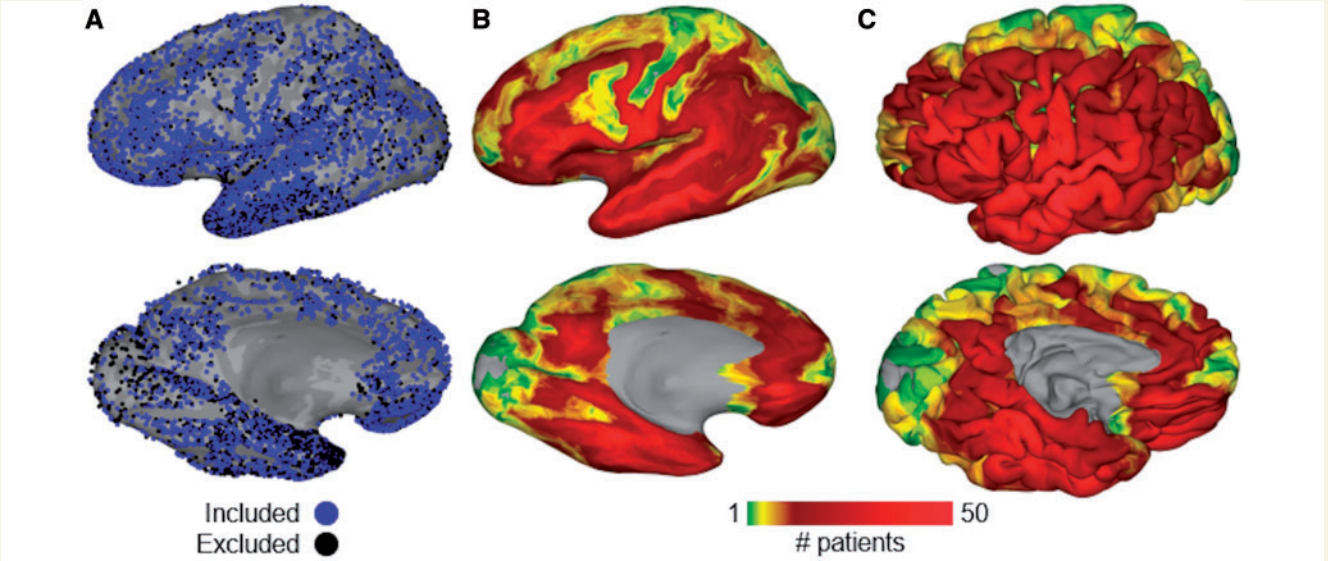

Figure 1 Group coverage map. (**A**) A total of 10 970 intracranial electrodes (5275 surface grids, 5696 depth probes) were implanted in 70 patients; 2857 were excluded (black) because of proximity to seizure onset sites, extrinsic noise, or right hemispheric language dominance. Electrodes are mapped to this common space by a surface-based transform to best match cortical topology across patients. (**B**) Aggregate of surface recording zones for all left hemisphere electrodes included in this study, shown on an inflated surface. (**C**) Same aggregate map, shown on the pial surface.

mean IQ 96 ± 14) by intra-carotid sodium amytal injection (Wada and Rasmussen, 2007) (n = 23), functional MRI laterality index (Ellmore *et al.*, 2010; Conner *et al.*, 2011) (n = 20), or the Edinburgh Handedness Inventory (Oldfield, 1971) (n = 21). Of the 64 patients with ECoG recordings used in this study, 57 patients completed both language tasks: picture naming and naming to definition. The remaining seven patients completed only one of these tasks (only naming to definition, n = 4; only picture naming, n = 3) due to time constraints. A total of 10 970 electrodes (5275 grid, 5696 depth) were implanted in this cohort. Of these, only the 8113 electrodes (3664 grid, 4449 depth) unaffected by epileptic activity, artefacts, or electrical noise were used in subsequent analyses (Fig. 1).

Experimental design

Patients engaged in visual and auditory cued naming tasks: picture naming and naming to definition (Fig. 2). They were instructed to name the object shown or described by the stimulus. Additionally, modality-specific control conditions were included for both tasks. The visual stimuli comprised of line drawings (Snodgrass and Vanderwart, 1980; Kaplan and Goodglass, 1983). The visual control condition comprised scrambled images produced by random rotation of pixel blocks; for these controls, patients were instructed to respond with 'scrambled'. The auditory stimuli were single sentence descriptions (average duration of 1.97 ± 0.36 s) recorded by both male and female speakers. These were designed such that the last word always contained crucial semantic information without which a specific response could not be generated (e.g. 'A round red *fruit*') (Hamberger and Seidel, 2003). The auditory control condition comprised of reversed speech to preserve the spectral content and amplitude envelope; for these controls, patients were asked to identify the gender of the speaker as either male or female.

During ECoG, patients were asked to articulate aloud the response to each stimulus. Visual stimuli were displayed on a 15" LCD screen positioned at eye-level for 1500 ms with an interstimulus interval of 3000 ms. The auditory stimuli were presented using stereo speakers (44.1 kHz, 15" MacBook Pro 2008) with an interstimulus interval of 5000 ms. A minimum of 120 visual (mean 289) and 70 auditory (mean 87) stimuli were presented to each patient using stimulus presentation software (Python v2.7).

During functional MRI, patients did not attempt overt articulation; instead, they pressed a button with the right thumb to indicate successful recall during task conditions and a separate button in response to control conditions. Visual stimuli were displayed for 1500 ms with an interstimulus interval of 515 ms. Auditory stimuli were played by stereo earbuds (100 Hz – 8 kHz flat bandwidth, 110 dB SPL) with a variable interstimulus interval of 515 ms. Each patient was presented with 160 pictures and auditory definitions along with 112 scrambled images and reversed speech samples. Identical stimulus presentation software was used for both the ECoG and functional MRI studies; the first 20 patients were presented with stimuli using Presentation (version 11, Neurobehavioral Systems) and the latter 44 patients using Python (version 2.7, www.python.org).

MRI acquisition

Preoperative anatomical MRI scans were obtained using a 3 T whole-body magnetic resonance scanner (Philips Medical Systems) fitted with a 16-channel SENSE head coil. Images were collected using a magnetization-prepared 180° radio-frequency pulse and rapid gradient-echo sequence with 1 mm sagittal slices and an in-plane resolution of 0.938 × 0.938 mm (Ellmore *et al.*, 2009). Pial surface reconstructions were computed with FreeSurfer (v5.1) (Dale *et al.*, 1999) and imported to AFNI (Cox, 1996). Postoperative CT scans were registered to the

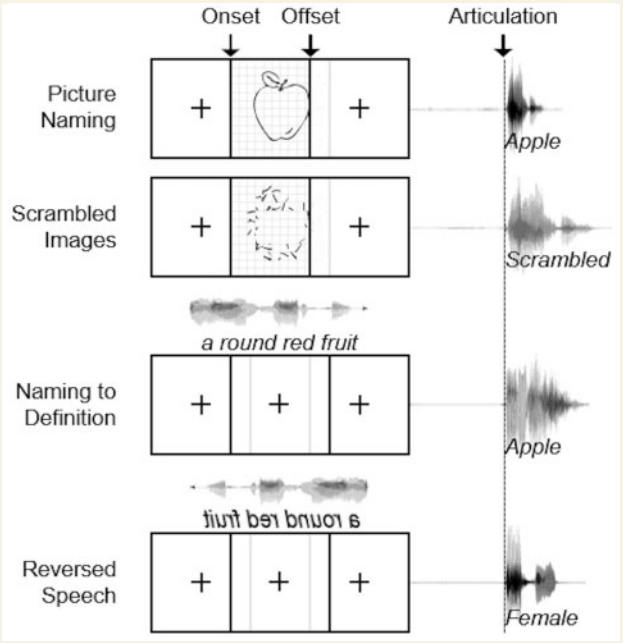

Figure 2 Experimental design. Schematic depiction of visual and auditory naming tasks with their respective control conditions. Visual stimuli were displayed for 1500 ms with a 3000 ms interstimulus interval. Auditory stimuli had an average length of 1970 ms with a 5000 ms interstimulus interval.

preoperative MRI scans to localize electrodes relative to cortex. Grid electrode locations were determined by a recursive grid partitioning technique and then optimized using intraoperative photographs (Pieters *et al.*, 2013). Depth electrode locations were informed by implantation trajectories from the ROSA surgical system.

Functional images were collected using a gradient-recalled echo-planar imaging sequence with 33 axial slices of 3 mm thickness and an in-plane resolution of 2.75 × 2.75 mm (echo time = 30 ms, repetition time = 2015 ms, flip angle = 90°). Stimuli were presented in a block design with two runs of each task (eight blocks each, 136 repetition time volumes, 20 s of task—picture naming or naming to definition, and 14 s of control—scrambled images or reversed speech) (Conner *et al.*, 2011). The presentation of visual stimuli and the initiation of auditory stimuli was coincident with the onset of each functional image volume.

Audio recordings and analysis

Continuous audio recordings of each patient were carried out during all experiments with an omnidirectional microphone (30–20 000 Hz response, 73 dB SNR, Audio Technica U841A) placed adjacent to the presentation laptop. These recordings were analysed offline to transcribe patient responses and select articulatory onset. Reaction times were measured as the interval from stimulus onset (visual tasks) or stimulus offset (auditory tasks) to the onset of articulation, accommodating distinct features of the visual and auditory stimuli.

ECoG acquisition

Grid electrodes—subdural platinum-iridium electrodes embedded in a silastic sheet (PMT Corporation; top-hat design; 3 mm diameter cortical contact)—were surgically implanted via a craniotomy following previously described methods (Tandon, 2008; Conner *et al.*, 2011; Pieters *et al.*, 2013). ECoG recordings were performed at least 2 days after the craniotomy to allow for recovery from the anaesthesia and narcotic medications. Depth stereo-electroencephalographic platinum-iridium electrodes (PMT Corporation; 0.8 mm diameter, 2.0 mm length cylinders; separated from adjacent contacts by 1.5–2.43 mm) were implanted using a Robotic Surgical Assistant (ROSA; Zimmer-Biomet) with stereotactic skull screws registered to both a CT angiogram and an anatomical MRI (Gonzalez-Martinez *et al.*, 2014, 2016). Each of these depth probes had 8–16 contacts and each patient had multiple (12–16) such probes implanted. Following surgical implantation, electrodes were localized using a procedure that involved registration of preoperative anatomical MRI and postoperative CT scans (Pieters *et al.*, 2013).

For the first 20 patients, ECoG data were collected with a 1000 Hz sampling rate and 0.15–300 Hz bandwidth using Neurofax (Nihon Kohden). For the latter 44 patients, data were collected with a 2000 Hz sampling rate and 0.1–700 Hz bandwidth using NeuroPort NSP (Blackrock Microsystems). Trials in which the patient answered incorrectly or did not respond were eliminated. Additionally, to minimize the effects of variance in reaction time between trials and across individuals, responses >2000 ms were removed (Conner *et al.*, 2014).

Digital signal processing

Analyses were performed with trials time-locked to stimulus onset, stimulus offset (only for the auditory task), and to response articulation. In all analyses, the baseline was defined prior to stimulus onset (−750 to −250 ms). Per cent change in power was calculated relative to this baseline. Line noise was removed with zero-phase second order Butterworth band-stop filters at 60 Hz and its first two harmonics. Spectrograms of individual trials (128-point Blackman window, 1024-point discrete Fourier transform) were averaged to generate a composite spectrogram of activity at each electrode. The gamma (60–120 Hz) analytic signal was generated from raw ECoG data by a frequency domain bandpass Hilbert filter (paired sigmoid flanks with half-width 1.5 Hz) (Bruns *et al.*, 2000; Conner *et al.*, 2014; Kadipasaoglu *et al.*, 2015; Whaley *et al.*, 2016).

Direct cortical stimulation and analysis

Language cortex was mapped as needed for clinical needs. Concurrent ECoG monitoring was carried out in all cases to detect any induced seizures. This procedure was conducted in 30 patients (23 with grid electrodes, seven with depth electrodes). Trains of 50 Hz balanced 0.3-ms period square-waves were delivered to adjacent electrodes for 3–5 s during the task (Tandon, 2012). Stimulation was applied using a Grass S88X Stimulator with a stimulus isolation unit (SIU) (Grass Technologies). At each electrode pair, stimulation was begun at a current of 2 mA and increased stepwise by 1 mA until

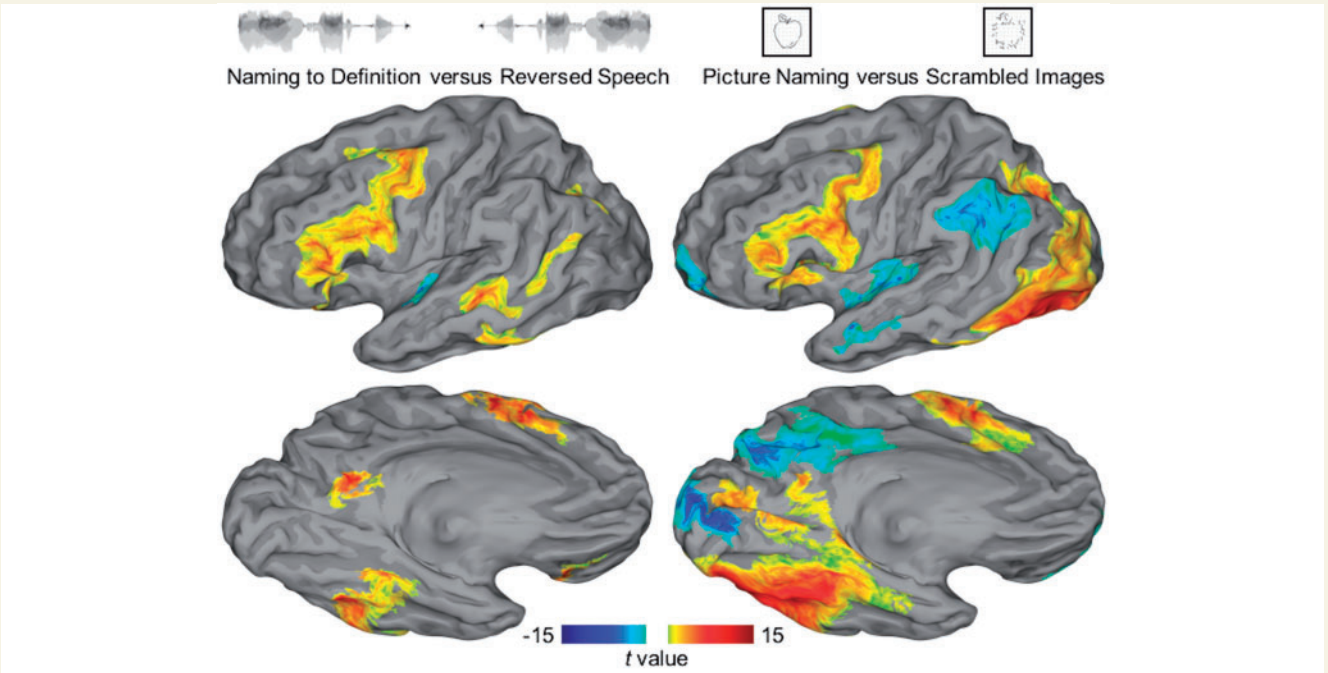

Figure 3 SB-MEMA of functional MRI. Surface-based group-level functional MRI represented on standard N27 surface. The contrast of auditory naming versus reversed speech is shown on the *left*; the contrast of picture naming versus scrambled images is shown on the *right*. Regions surviving a significance threshold ($P < 0.01$, corrected) are shown scaled by the model confidence—those with a preference for the semantic condition are shown in warm colours and for the control condition in cool colours.

either an overt phenomenon was observed, after-discharges were induced, or the 10-mA limit was reached. Stimulation sites were defined as positive for language tasks if stimulation resulted in articulation arrest or anomia. Furthermore, stimulation sites causing movement or sensation were separately recorded. Patient responses and behaviour were evaluated by clinical experts present in the room during the entire mapping session.

All electrodes mapped by direct cortical stimulation were co-localized using the same surface-based transform described previously (Fischl *et al.*, 1999) to generate a group coverage map of stimulated regions such that the value at each point on the group surface expresses the per cent of stimulations causing functional disruption. Regions with contributions from fewer than three patients were excluded from subsequent analysis.

Statistical analysis

To provide statistically robust and topologically precise estimates of BGA in ECoG and BOLD in functional MRI, population-level representations were created using surface-based mixed-effects multilevel analysis (SB-MEMA) (Fischl *et al.*, 1999; Chen *et al.*, 2012; Conner *et al.*, 2014; Kadipasaoglu *et al.*, 2014, 2015). Significance levels were computed at a corrected alpha-level of 0.01 using family-wise error rate corrections for multiple comparisons. The minimum criterion for the family-wise error rate was determined by white-noise clustering analysis (Monte Carlo simulations, 5000 iterations) of data with the same dimension and smoothness as that analysed (Kadipasaoglu *et al.*, 2014). Subsequently, a geodesic Gaussian smoothing filter (3 mm full-width at half-maximum) was applied. ECoG results were further restricted to regions with at least three patients contributing to coverage and BGA per cent change exceeding 5%.

Anatomical groups of electrodes were delineated with a two-step process. First, electrodes were indexed to the closest node on the standardized cortical surface (Saad and Reynolds, 2012). Second, anatomic centres and geodesic radii defined regions of interest by which to group electrodes for further analysis (Kadipasaoglu *et al.*, 2016; Whaley *et al.*, 2016). Group estimates of spectrotemporal response for a collection of electrodes were calculated by averaging across trials relative to articulation onset at each electrode, followed by an ensemble average across electrodes within each region. A Savitsky-Golay polynomial filter (third order, 251 ms frame length) was then applied to BGA traces. Parametric statistics were used as all regions contained >30 electrodes. To determine a significant increase in BGA from baseline, a two-sided paired *t*-test was evaluated at each time point for each region and significance levels were computed at a corrected alpha-level of 0.01 using the false discovery rate (FDR) correction for multiple comparisons. To determine a significant difference between conditions in the activation of a region, the cumulative BGA in a specified time window was evaluated with a two-sided paired *t*-test at an alpha-level of 0.01.

Results

Behavioural data

Reaction times during the control conditions were shorter than their object naming counterparts in both visual

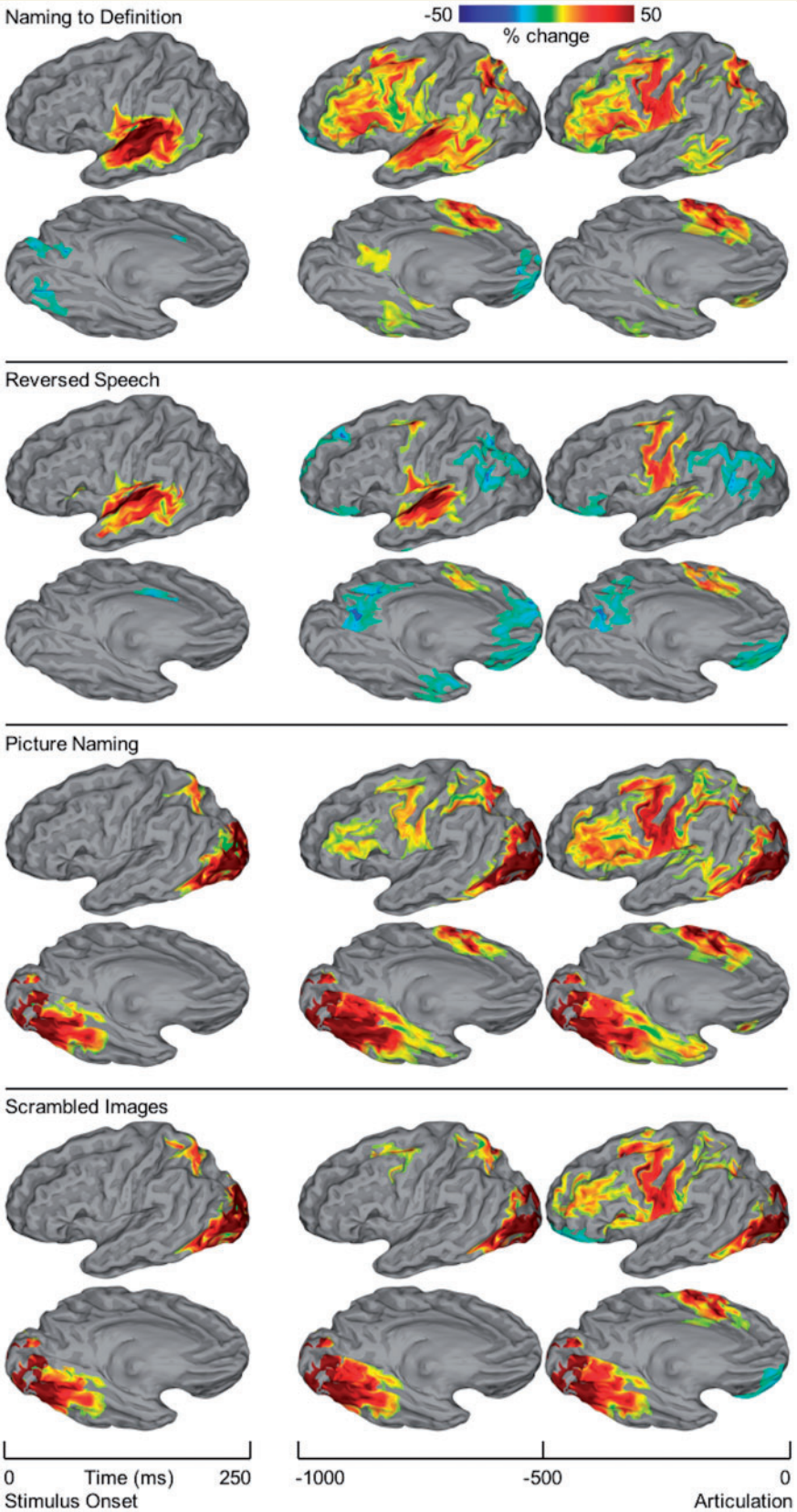

Figure 4 SB-MEMA of ECoG. Surface-based group-level ECoG represented on standard N27 surface. Rows are organized by condition: naming to definition; reversed speech; picture naming; scrambled images. Columns are organized by time windows aligned to either stimulus onset (250 ms width) or articulation (500 ms width). SB-MEMA maps estimate group BGA relative to baseline (−750 to −250 ms prestimulus). For each time window, the intersection of regions with significant activity ($P < 0.01$, corrected), absolute BGA change >5%, and coverage from at least three patients was computed. Confidence estimates from each map were corrected for multiple comparisons by excluding connected regions smaller than a fixed threshold empirically determined by white-noise clustering analysis. Two views are presented for each SB-MEMA map: lateral and ventral.

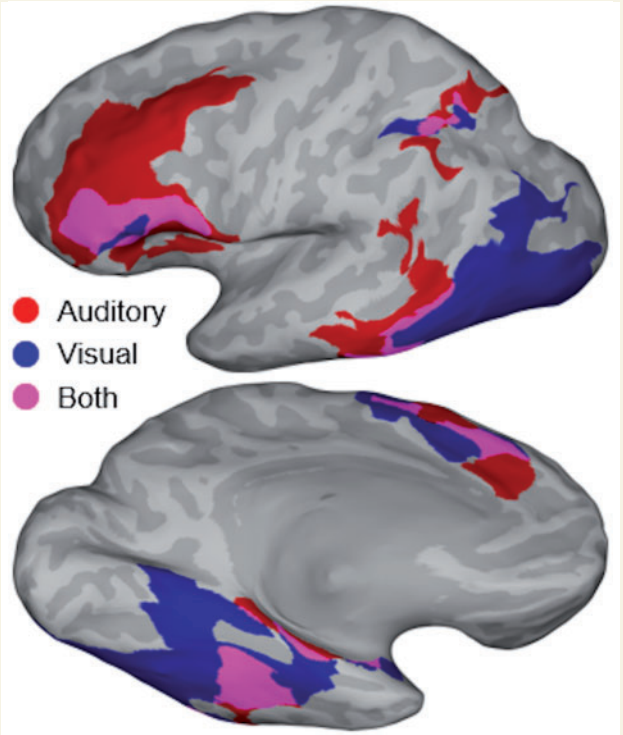

Figure 5 Heteromodal semantic contrast map. Conjunction of SB-MEMA maps aligned to articulation revealing heteromodal regions of semantic-specific BGA. SB-MEMA contrast maps were calculated for both auditory (naming to definition versus reversed speech) and visual (picture naming versus scrambled images) conditions. These pairs of maps were generated for 250 ms time windows in the full second preceding articulation (four total pairs). As in Fig. 4, binary thresholds were applied to each map based on effect estimate, corrected confidence, and electrode coverage. These resulting binary masks were combined via logical conjunction to generate the final conjunction map shown in this figure. Regions with semantic-specific activity in the full second preceding articulation are shown: visual domain, blue; auditory domain, red; both domains, purple.

(picture naming, 1252 ms; scrambled images, 1142 ms; paired *t*-test, $P = 10^{-9}$) and auditory tasks (naming to definition, 978 ms; reversed speech, 864 ms; paired *t*-test, $P = 10^{-5}$). The naming to definition task had faster reaction times than the picture naming task (paired *t*-test, $P = 10^{-24}$), likely due to the engagement of semantic and lexical networks prior to completion of the auditory stimulus (Friederici, 2002; Kotz *et al.*, 2002). Mean accuracy across all tasks was >90%; only trials with correct responses were analysed further.

Surface-based mixed-effects multilevel analysis

Two group analyses were performed—one of functional MRI data, the other of ECoG data—using SB-MEMA. The functional MRI maps contrast task versus control for both auditory and visual stimuli (Fig. 3). ECoG maps were computed separately for each condition relative to stimulus onset and articulation, revealing the temporal evolution of activity across the cortex (Fig. 4). Finally, a conjunction of task versus control contrasts from ECoG was generated to isolate areas with heteromodal BGA (Fig. 5). These analyses were repeated for the subgroup with all three data types: functional MRI, ECoG, and direct cortical stimulation (Supplementary Fig. 2 and Supplementary Table 2).

SB-MEMA of functional MRI in 36 patients (Fig. 3) revealed six distinct regions that demonstrate significantly enhanced BOLD signal during naming to definition compared to that during reversed speech: posterior middle temporal gyrus (pMTG), ventral temporal cortex (middle fusiform and inferior temporal gyri), intraparietal sulcus, precuneus, supplementary motor area (SMA), and inferior frontal gyrus (IFG). BOLD signal was also enhanced during picture naming in occipital cortex—terminating ventrally in middle fusiform gyrus, laterally in lateral occipital cortex, and dorsally in the intraparietal sulcus. Auditory and visual modalities showed overlapping regions of significance in middle fusiform gyrus, intraparietal sulcus, SMA, and IFG. These results are concordant with the conjunction of contrasts generated with ECoG (Fig. 5). Additionally, these results from a patient population with epilepsy did not differ from those seen in a normative population ($n = 21$, Supplementary Fig. 3). This is concordant with prior work that showed equivalent BOLD signal in diseased and normal populations (Conner *et al.*, 2014; Kadipasaoglu *et al.*, 2017), providing no evidence of a disease-induced remodelling of semantic memory organization.

SB-MEMA of ECoG in 61 patients (Fig. 4) during the auditory task revealed that early auditory cortex was active in the 250 ms after stimulus onset during both naming to definition and reversed speech. Naming to definition resulted in a greater magnitude and volume of activation in auditory sensory cortex than did reversed speech, consistent with the greater processing demands of phonologically structured stimuli (Hickok and Poeppel, 2007; Friederici, 2012; Chan *et al.*, 2014; Mesgarani *et al.*, 2014). BGA was concentrated in the early window (−1000 to −500 ms) preceding articulation at pMTG, ventral temporal cortex (middle fusiform and parahippocampal gyri), intraparietal sulcus, precuneus, middle frontal gyrus, and IFG (pars triangularis and opercularis). BGA peaked in the late window (−500 to 0 ms) preceding articulation at the SMA. Notably, no significant BGA was noted in the anterior fusiform gyrus or ventral temporal pole for any time window during naming to definition, despite significant coverage in these regions from 29 patients (Fig. 1).

SB-MEMA of ECoG in 60 patients during the visual task revealed that visual cortex was active in the 250 ms after stimulus onset for both picture naming and scrambled image conditions. This activity then spread along both ventral temporal and dorsal parietal streams. The ventral steam included the middle fusiform and parahippocampal gyri. BGA was greater for picture naming than scrambled images throughout fusiform gyrus, but this difference was

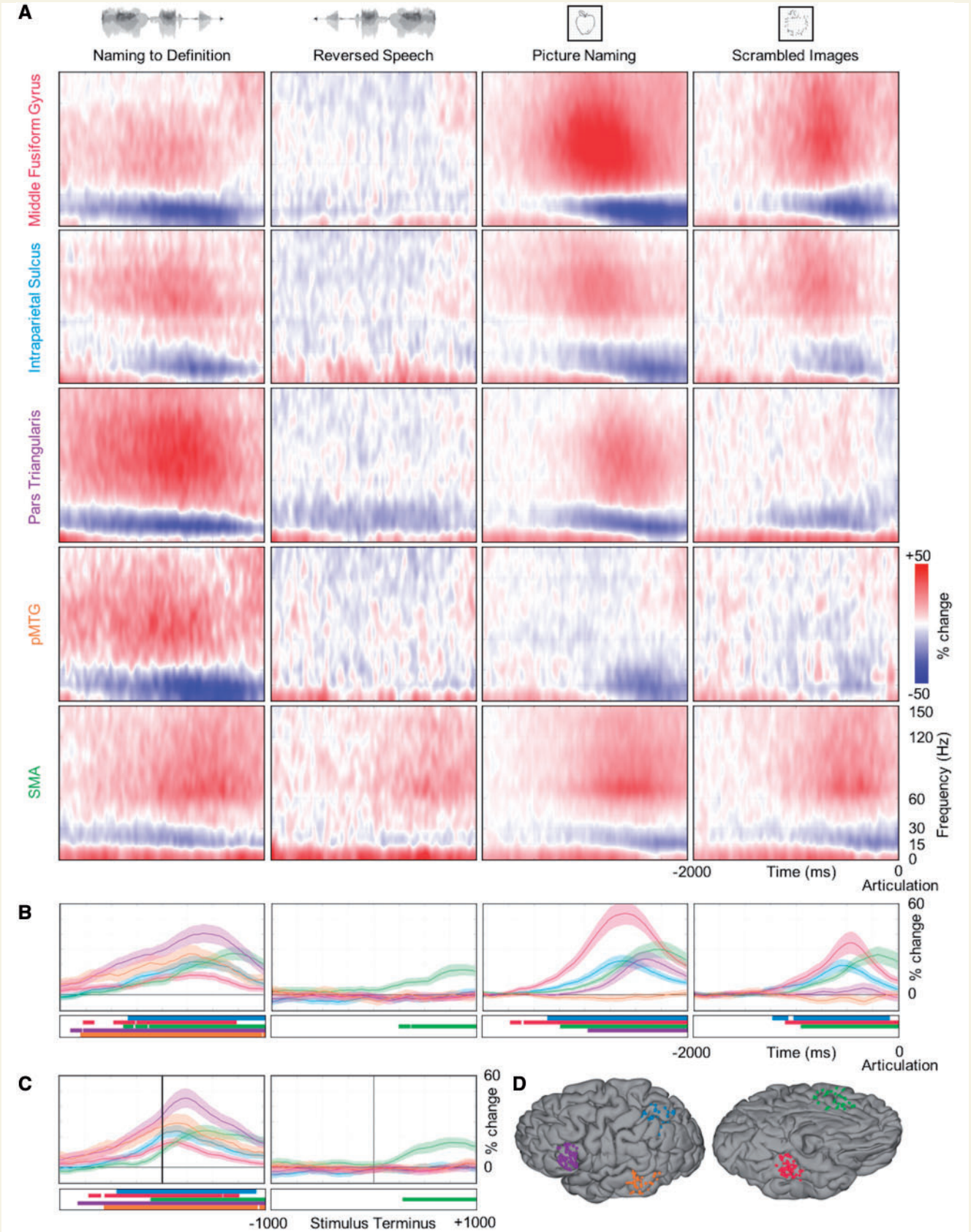

Figure 6 Temporal dynamics of lexical semantic network. Spectrotemporal responses at regions of interest. (**A**) Spectrograms show group estimates of the full spectrotemporal profile of each region (rows) in the 2 s before articulation for each condition (columns). (**B**) Time series show group estimates of BGA per cent change ± 1 standard error of the mean in the 2 s before articulation for each condition. Data are smoothed with a Savitsky-Golay filter (third order, 251 ms length). Significant increase from baseline is indicated by horizontal bars (paired *t*-test, $P < 0.01$, FDR corrected). (**C**) For the two auditory conditions, the same BGA estimates are shown aligned to the end of the stimulus. (**D**) Each anatomical region of interest is defined by a geodesic radius around a centre coordinate (Supplementary Table 1). All electrodes within each region are displayed on a standard N27 surface.

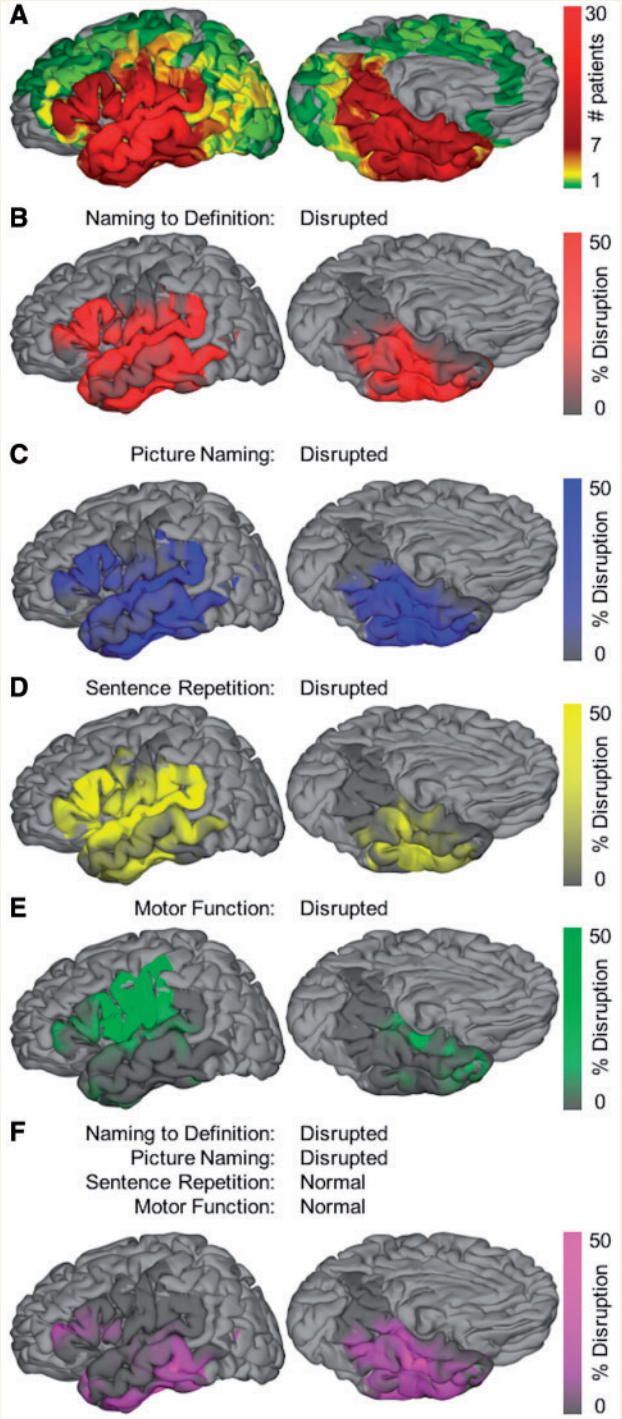

Figure 7 Stimulation language mapping. Surface-based group-level direct cortical stimulation represented on standard N27 surface. (**A**) Aggregate of the surface recording zones for all electrodes with direct cortical stimulation (subset of coverage map shown in Fig. 1). (**B**–**E**) Maps of per cent disruption for naming to definition, picture naming, sentence repetition, and motor function, respectively. Only cortex with at least three patients contributing to coverage is included in this analysis—the remaining cortex is shown in light grey. (**F**) Map for the conjunction of conditions: disrupted naming to definition and picture naming, intact sentence repetition and motor function. This isolates disruption that inhibits semantic access from disruption that inhibits articulatory function.

greatest in the anterior and lateral aspects—likely indexing the greater processing demands of coherent image features (Grill-Spector and Malach, 2004; Orban, 2008). Significant BGA in the ventral temporal pole was seen during picture naming immediately preceding articulation, while sub-threshold BGA was observed in scrambled images; however, the timing and distinct spectrotemporal fingerprint of this regional activity (Supplementary Fig. 1) reveal that this activity was an artefact generated by movement of the temporalis muscle (Otsubo *et al.*, 2008; Muthukumaraswamy, 2013). The dorsal stream included the intraparietal sulcus where BGA was greater during picture naming than scrambled images. In contrast to the ventral and dorsal visual processing pathways, activity in IFG and SMA was strongest in the late (−500 to 0 ms) window preceding articulation. As in the naming to definition task, middle frontal gyrus was recruited in parallel to IFG during both picture naming and scrambled image conditions.

To isolate activity specific to common semantic features from activity related to modality-specific sensory processing or to articulation, we performed a conjunction of two contrasts: [naming to definition versus reversed speech] + [picture naming versus scrambled images] in the 1000 ms preceding articulation. Activity in four regions was enhanced for both auditory and visual semantic contrasts: the middle fusiform gyrus, intraparietal sulcus, SMA, and IFG (Fig. 5). Notably, there was no significant intersection of these heteromodal semantic contrasts in pMTG—the activity here was uniquely enhanced during the naming to definition task, while activity in lateral occipital cortex was uniquely enhanced during the picture naming task.

Regional spectrotemporal responses

To resolve the timing of distributed activity across the heteromodal lexical semantic network, we targeted the five regions—middle fusiform gyrus, the intraparietal sulcus, pars triangularis, pMTG, and SMA (Fig. 6D)—identified by the convergent evidence from surface-based group analyses of functional MRI and ECoG data. Each region was well-sampled (minimum of 67 electrodes) (Supplementary Table 1). The group spectrograms derived from all of the electrodes in a region manifested a consistent spectrotemporal fingerprint with three primary characteristics: a low frequency (< 10 Hz) power increase that preceded a coincident beta (15–30 Hz) power decrease and gamma (> 30 Hz) power increase (Fig. 6A).

Naming to definition induced BGA greater than that during reversed speech in four regions that peaked prior to articulation (Fig. 6B): pMTG at −731 ms, middle fusiform gyrus at −724 ms, intraparietal sulcus at −658 ms, and pars triangularis at −597 ms. When aligned to the end of the auditory stimulus, these regions all showed peak activity after the auditory stimuli had finished (Fig. 6C): pMTG at +139 ms, middle fusiform at +143 ms, intraparietal sulcus at +156 ms, and pars triangularis at +240 ms. Crucially, none

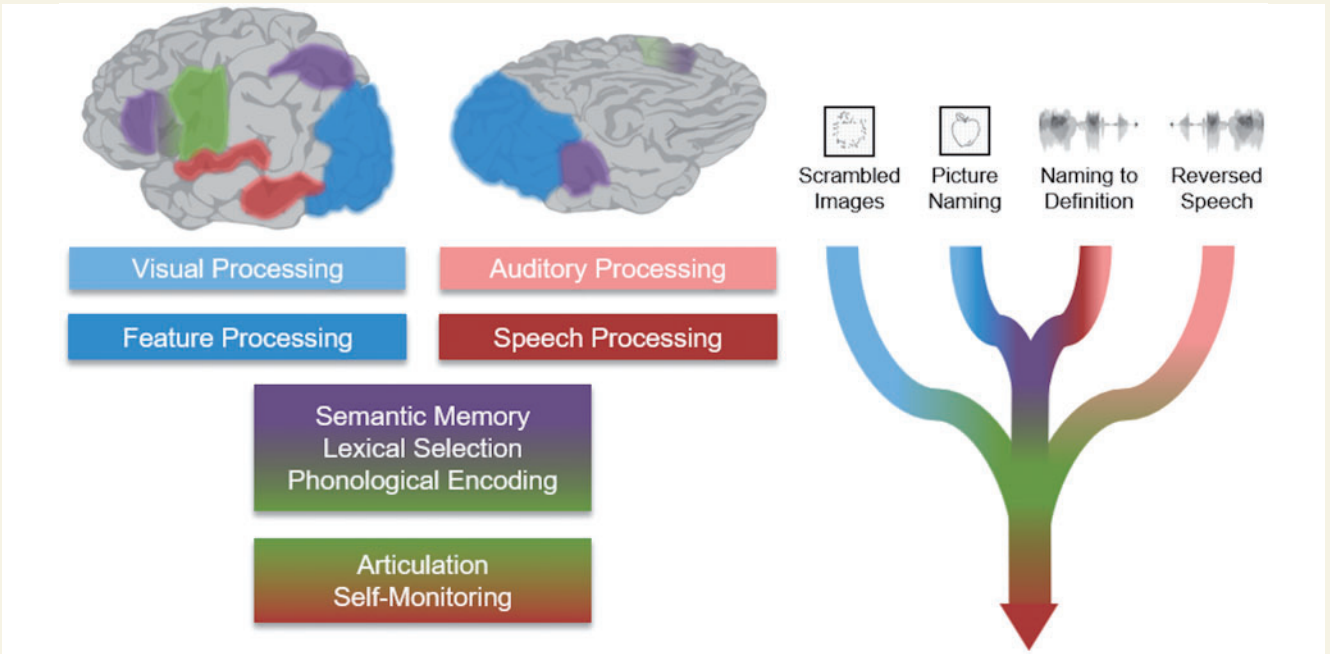

Figure 8 Theoretic schematic. Schematic description of heteromodal cued naming tasks. The pair of lead-in processes converge in a shared lexical semantic network, which ultimately drives articulation. The control tasks—scrambled images and reversed speech—do not require higher sensory processing or engagement of lexical semantic faculties.

of these four regions showed significant activity during the first half of the naming to definition stimuli—the cortical response was strongly tied to the terminus of the spoken sentence. The SMA produced significant BGA during both the naming to definition and reversed speech conditions with peak activity at −315 ms and −107 ms relative to articulation onset, respectively; however, BGA was also significantly greater in SMA for naming to definition than in reversed speech during the 1000 ms preceding articulation ($P = 0.0042$). This increased activity reflects the greater articulatory needs of varying—as opposed to stereotyped 'male' or 'female'—responses.

Picture naming induced BGA greater than that for scrambled images in three regions that peaked prior to articulation (Fig. 6B): middle fusiform gyrus at −595 ms, intraparietal sulcus at −626 ms, and pars triangularis at −395 ms. Middle fusiform gyrus showed significant BGA for both picture naming and scrambled images; however, BGA was also significantly greater for picture naming than for scrambled images during the 1000 ms preceding articulation (53.73%, 34.32%, $P = 0.004$). The intraparietal sulcus showed significant BGA for both picture naming and scrambled images; BGA was not significantly greater for picture naming than for scrambled images during the 1000 ms preceding articulation (22.38%, 19.34%, $P = 0.2805$). Pars triangularis exhibited significant BGA only for picture naming—no significant BGA was observed for scrambled images. BGA in pMTG was notably absent during picture naming in comparison with naming to definition; instead, there was significant beta suppression in the 1000 ms preceding articulation for picture naming ($P = 0.0052$), but not for scrambled images ($P = 0.6418$). During the visual conditions, activity in the SMA showed a similar pattern as observed in the auditory conditions. There was significant BGA during both picture naming and scrambled images with peak activity at −274 ms and −190 ms relative to articulation onset, respectively; however, there was no significant difference in BGA between these conditions at any point during the 1000 ms preceding articulation (29.91%, 26.42%, $P = 0.2510$).

We also investigated the spectrotemporal response of sensory processing and sensorimotor regions (Supplementary Fig. 1). As expected, early sensory cortices showed modality-specific lead-in processes to semantic access that were similar for both task and control conditions (Indefrey and Levelt, 2004). Early auditory cortex manifested significant BGA for the duration of the naming to definition and the reversed speech stimuli with no significant difference between task and control in the −2000 to −1000 ms interval relative to articulation ($P = 0.0547$). Early visual cortex manifested BGA throughout the presentation of both pictures and scrambled images with no significant difference between task and control in the 2000 ms preceding articulation ($P = 0.8584$). These lead-in processes converge in the lexical semantic network, which subsequently engages a shared system for articulation (Fig. 8). In all four conditions, mouth sensorimotor cortex in subcentral gyrus showed significant BGA that peaked around articulation onset (naming to definition, 82.34%, +59 ms; reversed speech, 78.70%, +69 ms; picture naming, 94.13%, +114 ms; scrambled images, 94.73%, +49 ms).

Finally, we also investigated the spectrotemporal response of ventral temporal pole (Supplementary Fig. 1)—a region that has garnered attention in prior studies (Patterson *et al.*, 2007; Ralph *et al.*, 2016). BGA in the ventral temporal pole was similar in all four conditions and well-aligned with activity in sensorimotor cortex. Importantly, this activity is much later than that of middle fusiform gyrus, the intraparietal sulcus, IFG and pMTG (Fig. 6B). The ventral temporal pole—well sampled in our cohort (104 electrodes in 29 patients)—showed an unusual spectrotemporal fingerprint with a strong power modulation in very high frequencies (>120 Hz) and a consistent alignment with articulatory onset (Supplementary Fig. 4). Given the proximity of this cortical region with the temporalis muscle, this activity likely reflects an artefact of movement related to articulation (Otsubo *et al.*, 2008; Muthukumaraswamy, 2013).

Taken together, three stages of cortical activity in the left hemisphere are revealed by these analyses. Initially, sensory cortex (auditory or visual) is activated in response to an external stimulus to generate higher-order representation, e.g. phonology or shape, respectively. Next, a distributed network comprising three nodes is selectively engaged if there is a semantic memory load: middle fusiform gyrus, intraparietal sulcus, and pars triangularis. Lastly, regions explicitly supporting articulation are engaged immediately preceding the generation of an object name.

Direct cortical stimulation

BGA derived from ECoG provides correlative—but not causal—evidence for the engagement of specific regions in a cognitive process; in contrast, transient lesions induced by direct cortical stimulation provide a direct causal measure of cognitive disruption. We compared the functional maps of lexical semantic processing from functional MRI and ECoG with language disruption from direct cortical stimulation in 30 of these patients (Fig. 7A), 23 with grid electrodes and seven with depth electrodes. Mapping was performed in each case to support clinical decision-making and was therefore focused primarily on lateral temporal, inferior frontal, and ventral temporal cortex.

Stimulation-positive sites (i.e. sites where stimulation caused a functional deficit) specific for naming to definition were principally localized to lateral temporal cortex (Fig. 7B). Those specific for picture naming were predominantly located in posterior ventral temporal cortex (Fig. 7C). Sentence repetition was primarily disrupted by peri-Sylvian stimulation (Fig. 7D). Motor positive sites were tightly localized to pars opercularis and ventral sensorimotor cortex (Fig. 7E).

To isolate cortical regions where stimulation disrupted semantic processing irrespective of modality, we performed a conjunction of these functional maps: [positive for picture naming and naming to definition] + [negative for sentence repetition and sensorimotor effects] (Fig. 7F). This revealed two loci. The first locus was the middle fusiform gyrus, which has also been characterized as the basal temporal language area (Burnstine *et al.*, 1990; Lüders *et al.*, 1991). This region was well-aligned with the corresponding functional locus observed in both functional MRI (Fig. 3) and ECoG (Fig. 5). The second locus was pMTG, overlapping with the corresponding functional locus defined by the contrast of naming to definition and reversed speech; however, this region does not show increased functional activity for picture naming or scrambled images.

Discussion

There is accumulating evidence for the involvement of ventral temporal cortex in semantic memory from neuropsychological studies (Warrington, 1975; Nestor *et al.*, 2006), electrical stimulation of cortex (Burnstine *et al.*, 1990; Lüders *et al.*, 1991), PET (Damasio *et al.*, 1996; Noppeney and Price, 2002; Bright *et al.*, 2004; Sharp *et al.*, 2004; Spitsyna *et al.*, 2006), magnetoencephalography (Marinkovic *et al.*, 2003), and intracranial event-related potentials (Nobre *et al.*, 1994; Liu *et al.*, 2009). These studies broadly implicate the entire ventral surface from the temporal pole through the fusiform gyrus. A consensus on the focal neurobiological substrate underlying a lexical semantic hub in ventral temporal cortex has yet to emerge (Ralph *et al.*, 2016). Furthermore, a number of recent influential reviews disregard this region and assign semantic function solely to lateral regions (Mesulam, 1998; Thompson-Schill, 2003; Catani and Ffytche, 2005; Martin, 2007).

We studied object naming using three complementary methodologies: functional MRI ($n = 36$), ECoG ($n = 64$), and direct cortical stimulation ($n = 30$) during both auditory verbal and visual non-verbal stimuli, each paired with a modality-specific nonsense control. Large-scale integrated ECoG combining both surface and depth electrodes is particularly well-suited for the study of distributed language networks given the complete coverage of the cortical surface with high spatiotemporal resolution. These data provide compelling large-scale evidence for audio-visual cortex supporting semantic cognition in the middle fusiform gyrus.

The ventral temporal lobe is especially at risk in surgical approaches for mesial temporal lobe epilepsy. A major advantage of newer minimally invasive approaches, such as laser interstitial thermal ablation, is the reduction of cognitive deficits, particularly naming, for epilepsy in the language-dominant hemisphere. The fact that the middle fusiform cortex is typically spared in such approaches supports its role in semantic memory (Drane *et al.*, 2015; Hoppe *et al.*, 2017).

Serial stages in object naming

We found that three stages of activity during both naming to definition and picture naming followed a serial

progression with clear functional specialization (Indefrey and Levelt, 2004): sensory processing, semantic processing, and articulation (Fig. 8). These stages were distinguished by consistent spatiotemporal patterns of BGA activity prior to articulation.

The location and timing of primary sensory processing was modality-dependent. During the naming to definition stimulus, auditory cortex involved in sentence comprehension was active throughout—consistent with the role of STG in language-specific feature extraction, superior temporal sulcus in phonological processing, and pMTG in lexical access (Hickok and Poeppel, 2004, 2007). In contrast, activation after presentation of the visual stimulus began in the early visual cortex and spread forward along the two hierarchical visual processing streams (Ungerleider and Mishkin, 1982; Felleman and Van Essen, 1991): ventral, caudal to rostral fusiform gyrus; dorsal, occipital pole to the intraparietal sulcus.

Following feature extraction in sensory cortex, concurrent activity was notable in a specific set of distributed regions for both naming to definition and picture naming, but not for reversed speech or scrambled images: middle fusiform gyrus, the intraparietal sulcus, IFG, and SMA. Except for the SMA, activity in these heteromodal semantic-specific regions preceded sensorimotor cortex activity corresponding to the third stage—articulatory planning. The spatiotemporal activation profiles suggest a three-locus network for lexical semantic processing: the middle fusiform gyrus, the intraparietal sulcus, and IFG. Notably, the pMTG and temporal pole were not engaged in this process.

The final stage—articulation—was similar across all four conditions during ECoG recordings. The SMA led activity in the articulatory network, followed by mouth sensorimotor cortex and early auditory cortex. Direct stimulation of temporal cortex spanning STG to the Sylvian parietal temporal junction disrupted naming to definition, picture naming, as well as sentence repetition. The same pattern was observed in pars triangularis. Stimulation of pars opercularis and of sensorimotor cortex disrupted motor function (Hickok and Poeppel, 2007; Hickok *et al.*, 2011; Hickok, 2012).

Semantic selection

The IFG is widely accepted to be involved in semantic selection and phonological processing functions (Thompson-Schill *et al.*, 1997; Wagner *et al.*, 2001; Hickok and Poeppel, 2007), which are thought to be segregated along an anterior-posterior axis (Poldrack *et al.*, 1999; Badre *et al.*, 2005). In this study, population maps from both functional MRI and ECoG revealed that the IFG was the frontal lobe region coactive for semantic contrasts in both sensory modalities. Furthermore, disruption of this region with direct cortical stimulation resulted in heteromodal naming deficits. These deficits were also seen with stimulation during a sentence repetition task, emphasizing the role of the IFG as an interface between lexical semantic and articulatory networks. These results are consistent with pars triangularis exerting top-down control over the semantic network, perhaps with feedforward and feedback information encoded within distinct frequency bands (Bastos *et al.*, 2015; Michalareas *et al.*, 2016).

Semantic encoding

The ventral temporal cortex has been a region of interest in semantic memory since early studies of semantic dementia identified patients with intact sensory processing and deficits in conceptual knowledge (Warrington, 1975). Studies in non-human primates reveal that large numbers of auditory and visual fibres converge at the temporal pole (Morán *et al.*, 1987; Felleman and Van Essen, 1991), suggesting that this region may also be an integrative locus. Subsequently, studies of direct cortical stimulation revealed that disruption of the basal temporal language area—defined as fusiform gyrus within 30–70 mm of the temporal pole—results in speech arrest (Lüders *et al.*, 1991). This effect was also observed following stimulation of parahippocampal gyrus and anterior inferior temporal gyrus (Burnstine *et al.*, 1990). PET studies provided the first observations of functional activity in the ventral temporal cortex to both visual and auditory stimuli (Nobre *et al.*, 1994; Damasio *et al.*, 1996; Marinkovic *et al.*, 2003; Spitsyna *et al.*, 2006; Xu *et al.*, 2009). The atrophy and hypometabolism observed in semantic dementia has been localized to the anterior fusiform gyrus (Binney *et al.*, 2010; Mion *et al.*, 2010).

We identified four regions with activity common to semantic conditions: middle fusiform gyrus, the intraparietal sulcus, SMA, and IFG. The timing of SMA activity suggests a role in early articulatory planning while IFG interfaces between lexical semantic and phonological networks. This suggests that the remaining two regions—middle fusiform gyrus and the intraparietal sulcus—are critical for semantic encoding. The spatial extent of significant BOLD signal found with functional MRI and significant BGA found with ECoG were well-aligned. Direct cortical stimulation of ventral temporal cortex revealed a middle fusiform region that produced heteromodal naming deficits. This region was slightly anterior to that identified by functional activity, but both were well within the bounds of the basal temporal language area (Burnstine *et al.*, 1990; Lüders *et al.*, 1991). The functional activity identified by functional MRI and ECoG showed less substantial heteromodal overlap in the intraparietal sulcus than was found in the middle fusiform gyrus. This could be due to the focus in this study on common object naming as opposed to action naming, which may recruit parietal regions more strongly (Chao and Martin, 2000; Binder and Desai, 2011; Conner *et al.*, 2014).

The data do not support that the activity in middle fusiform gyrus and the intraparietal sulcus represents ancillary 'visual imagery' (Mellet *et al.*, 1998; Ishai *et al.*, 2000;

Ganis *et al.*, 2004). First, the timing of activity in these regions shows that they engage only at the end of the auditory stimulus. Despite the serial presentation of evocative descriptors in the naming to definition task, no visual imagery occurs until its completion. Second, direct stimulation to this region causes heteromodal naming deficits—incongruous for a region performing a facultative process.

Negative results

Several prominent theories hold that pMTG is a central site for semantic representation (Martin, 2007), a secondary region engaged with IFG in semantic control (Noppeney *et al.*, 2004; Badre *et al.*, 2005), or a lexical interface (Hickok and Poeppel, 2007). Using both functional MRI and ECoG, only naming to definition against reversed speech produced a significant semantic contrast in pMTG; however, direct cortical stimulation at pMTG disrupted both naming to definition and picture naming. These results are most consistent with lexical processing at pMTG.

Neuropsychological studies suggest a key role of the temporal pole in heteromodal semantic processing. With three distinct methods, we demonstrate no semantic-specific activity in the ventral temporal pole for either naming to definition or picture naming. First, no significant BOLD signal is reported in either functional MRI semantic contrast. Second, ECoG further reveals that the observed artefact in ventral temporal pole is well-aligned with articulation and best explained by temporalis muscle movement (Otsubo *et al.*, 2008; Muthukumaraswamy, 2013). Third, direct cortical stimulation of the temporal pole does not disrupt either naming to definition or picture naming. The evidence presented here strongly suggests that the temporal pole does not support semantic memory for objects.

Conclusion

With large-scale functional MRI and ECoG, significant and robust semantic-specific BOLD signal and BGA common for auditory and visual modalities was seen only in middle fusiform gyrus and IFG. Analysis of group-level interregional temporal dynamics revealed a consistent progression through three stages during object naming: primary sensory processing, semantic processing, and articulatory planning. The second of these stages was absent during the non-semantic control conditions in both sensory modalities. Direct cortical stimulation also identified a region in middle fusiform gyrus that consistently disrupted both picture naming and naming to definition, but not downstream articulatory processes. Altogether, these results demonstrate that auditory and visual features processed in distinct sensory cortices converge in a shared lexical semantic network—including middle fusiform gyrus—prior to articulation.

Acknowledgements

We thank all the patients who participated in this study; laboratory members at the Tandon lab (Thomas Pieters, Vatche Baboyan, Patrick Rollo, Matthew Rollo and Jessica Johnson); neurologists at the Texas Comprehensive Epilepsy Program (Jeremy Slater, Giridhar Kalamangalam, Omotola Hope, Melissa Thomas) who participated in the care of these patients; and all the nurses and technicians in the Epilepsy Monitoring Unit at Memorial Hermann Hospital who helped make this research possible.

Funding

This work was supported by the National Institute for Deafness and other Communication Disorders DC014589, National Center for Research Resources Clinical and Translational Award K12-KL2 RR0224149, and the Memorial Hermann Foundation.

Supplementary material

Supplementary material is available at *Brain* online.

References

Badre D, Poldrack RA, Paré-Blagoev EJ, Insler RZ, Wagner AD. Dissociable controlled retrieval and generalized selection mechanisms in ventrolateral prefrontal cortex. Neuron 2005; 47: 907–18.

Bastos AM, Vezoli J, Bosman CA, Schoffelen JM, Oostenveld R, Dowdall JR, et al. Visual areas exert feedforward and feedback influences through distinct frequency channels. Neuron 2015; 85: 390–401.

Binder JR, Desai RH. The neurobiology of semantic memory. Trends Cogn Sci 2011; 15: 527–36.

Binder JR, Desai RH, Graves WW, Conant LL. Where is the semantic system? A critical review and meta-analysis of 120 functional neuroimaging studies. Cereb Cortex 2009; 19: 2767–96.

Binney RJ, Embleton KV, Jefferies E, Parker GJ, Ralph MA. The ventral and inferolateral aspects of the anterior temporal lobe are crucial in semantic memory: evidence from a novel direct comparison of distortion-corrected fMRI, rTMS, and semantic dementia. Cereb Cortex 2010; 20: 2728–38.

Bright P, Moss H, Tyler LK. Unitary vs multiple semantics: PET studies of word and picture processing. Brain Lang 2004; 89: 417–32.

Brown R, McNeill D. The "tip of the tongue" phenomenon. J Verbal Learning Verbal Behav 1966; 5: 325–37.

Bruns A, Eckhorn R, Jokeit H, Ebner A. Amplitude envelope correlation detects coupling among incoherent brain signals. Neuroreport 2000; 11: 1509–14.

Burnstine TH, Lesser RP, Hart J, Uematsu S, Zinreich SJ, Krauss GL, et al. Characterization of the basal temporal language area in patients with left temporal lobe epilepsy. Neurology 1990; 40: 966–70.

Cardin JA, Carlén M, Meletis K, Knoblich U, Zhang F, Deisseroth K, et al. Driving fast-spiking cells induces gamma rhythm and controls sensory responses. Nature 2009; 459: 663–7.

Catani M, Ffytche DH. The rises and falls of disconnection syndromes. Brain 2005; 128: 2224–39.

Chan AM, Dykstra AR, Jayaram V, Leonard MK, Travis KE, Gygi B, et al. Speech-specific tuning of neurons in human superior temporal gyrus. Cereb Cortex 2014; 24: 2679–93.
Chao LL, Martin A. Representation of manipulable man-made objects in the dorsal stream. Neuroimage 2000; 12: 478–84.
Chen G, Saad ZS, Nath AR, Beauchamp MS, Cox RW. FMRI group analysis combining effect estimates and their variances. Neuroimage 2012; 60: 747–65.
Conner CR, Chen G, Pieters TA, Tandon N. Category specific spatial dissociations of parallel processes underlying visual naming. Cereb Cortex 2014; 24: 2741–50.
Conner CR, Ellmore TM, Pieters TA, DiSano MA, Tandon N. Variability of the relationship between electrophysiology and BOLD-fMRI across cortical regions in humans. J Neurosci 2011; 31: 12855–65.
Cox RW. AFNI: software for analysis and visualization of functional magnetic resonance neuroimages. Comput Biomed Res 1996; 29: 162–73.
Crone NE, Hao L, Hart J, Boatman D, Lesser RP, Irizarry R, et al. Electrocorticographic gamma activity during word production in spoken and sign language. Neurology 2001; 57: 2045–53.
Dale AM, Fischl B, Sereno MI. Cortical surface-based analysis. I. Segmentation and surface reconstruction. Neuroimage 1999; 9: 179–94.
Damasio H, Grabowski TJ, Tranel D, Hichwa RD, Damasio AR. A neural basis for lexical retrieval. Nature 1996; 380: 499–505.
Devlin JT, Russell RP, Davis MH, Price CJ, Wilson J, Moss HE, et al. Susceptibility-induced loss of signal: comparing PET and fMRI on a semantic task. Neuroimage 2000; 11: 589–600.
Drane DL, Loring DW, Voets NL, Price M, Ojemann JG, Willie JT, et al. Better object recognition and naming outcome with MRI-guided stereotactic laser amygdalohippocampotomy for temporal lobe epilepsy. Epilepsia 2015; 56: 101–13.
Ellmore TM, Beauchamp MS, O'Neill TJ, Dreyer S, Tandon N. Relationships between essential cortical language sites and subcortical pathways. J Neurosurg 2009; 111: 755–66.
Ellmore TM, Beauchamp MS, Breier JI, Slater JD, Kalamangalam GP, O'Neill TJ, et al. Temporal lobe white matter asymmetry and language laterality in epilepsy patients. Neuroimage 2010; 49: 2033–44.
Felleman DJ, Van Essen DC. Distributed hierachical processing in the primate cerebral cortex. Cereb Cortex 1991; 1: 1–47.
Fischl B, Sereno MI, Tootell RB, Dale AM. High-resolution inter-subject averaging and a surface-based coordinate system. Hum Brain Mapp 1999; 8: 272–84.
Friederici AD. Towards a neural basis of auditory sentence processing. Trends Cogn Sci 2002; 6: 78–84.
Friederici AD. The cortical language circuit: from auditory perception to sentence comprehension. Trends Cogn Sci 2012; 16: 262–8.
Ganis G, Thompson WL, Kosslyn SM. Brain areas underlying visual mental imagery and visual perception: an fMRI study. Cogn Brain Res 2004; 20: 226–41.
Gonzalez-Martinez J, Bulacio J, Thompson S, Gale J, Smithason S, Najm I, et al. Technique, results, and complications related to robot-assisted stereoelectroencephalography. Neurosurgery 2016; 78: 169–80.
Gonzalez-Martinez J, Mullin J, Vadera S, Bulacio J, Hughes G, Jones S, et al. Stereotactic placement of depth electrodes in medically intractable epilepsy. J Neurosurg 2014; 120: 639–44.
Grill-Spector K, Malach R. The human visual cortex. Annu Rev Neurosci 2004; 27: 649–77.
Hamberger MJ, Seidel WT. Auditory and visual naming tests: normative and patient data for accuracy, response time, and tip-of-the-tongue. J Int Neuropsychol Soc 2003; 9: 479–89.
Hansen P, Kringelbach M, Salmelin R. MEG: an introduction to methods. New York: Oxford University Press; 2010.
Hickok G. The cortical organization of speech processing: feedback control and predictive coding the context of a dual-stream model. J Commun Disord 2012; 45: 393–402.
Hickok G, Houde J, Rong F. Sensorimotor integration in speech processing: computational basis and neural organization. Neuron 2011; 69: 407–22.
Hickok G, Poeppel D. Dorsal and ventral streams: a framework for understanding aspects of the functional anatomy of language. Cognition 2004; 92: 67–99.
Hickok G, Poeppel D. The cortical organization of speech processing. Nat Rev Neurosci 2007; 8: 393–402.
Hoppe C, Witt JA, Helmstaedter C, Gasser T, Vatter H, Elger CE. Laser interstitial thermotherapy (LiTT) in epilepsy surgery. Seizure 2017; 48: 45–52.
Indefrey P, Levelt WJM. The spatial and temporal signatures of word production components. Cognition 2004; 92: 101–44.
Ishai A, Ungerleider LG, Haxby JV. Distributed neural systems for the generation of visual images. Neuron 2000; 28: 979–90.
Jacobs J, Kahana MJ. Direct brain recordings fuel advances in cognitive electrophysiology. Trends Cogn Sci 2010; 14: 162–71.
Kadipasaoglu CM, Baboyan VG, Conner CR, Chen G, Saad ZS, Tandon N. Surface-based mixed effects multilevel analysis of grouped human electrocorticography. Neuroimage 2014; 101: 215–24.
Kadipasaoglu CM, Conner CR, Baboyan VG, Rollo M, Pieters TA, Tandon N. Network dynamics of human face perception. PLoS One 2017; 12: e0188834.
Kadipasaoglu CM, Conner CR, Whaley ML, Baboyan VG, Tandon N. Category-selectivity in human visual cortex follows cortical topology: a grouped icEEG study. PLoS One 2016; 11: e0157109.
Kadipasaoglu CM, Forseth K, Whaley M, Conner CR, Rollo MJ, Baboyan VG, et al. Development of grouped icEEG for the study of cognitive processing. Front Psychol 2015; 6: 1008.
Kaplan E, Goodglass H, Weintraub S. The Boston naming test. Philadelphia: Lea and Febiger. 1983.
Kotz SA, Cappa SF, von Cramon DY, Friederici AD. Modulation of the lexical-semantic network by auditory semantic priming: an event-related functional MRI study. Neuroimage 2002; 17: 1761–72.
Lachaux JP, Axmacher N, Mormann F, Halgren E, Crone NE. High-frequency neural activity and human cognition: past, present and possible future of intracranial EEG research. Prog Neurobiol 2012; 98: 279–301.
Liu H, Agam Y, Madsen JR, Kreiman G. Timing, timing, timing: fast decoding of object information from intracranial field potentials in human visual cortex. Neuron 2009; 62: 281–90.
Logothetis NK. The underpinnings of the BOLD functional magnetic resonance imaging signal. J Neurosci 2003; 23: 3963–71.
Lüders H, Lesser RP, Hahn J, Dinner DS, Morris HH, Wyllie E, et al. Basal temporal language area. Brain 1991; 114 (Pt 2): 743–54.
Magri C, Schridde U, Murayama Y, Panzeri S, Logothetis NK. The amplitude and timing of the BOLD signal reflects the relationship between local field potential power at different frequencies. J Neurosci 2012; 32: 1395–407.
Manning JR, Jacobs J, Fried I, Kahana MJ. Broadband shifts in local field potential power spectra are correlated with single-neuron spiking in humans. J Neurosci 2009; 29: 13613–20.
Margolin DI, Pate DS, Friedrich FJ, Elia E. Dysnomia in dementia and in stroke patients: different underlying cognitive deficits. J Clin Exp Neuropsychol 1990; 12: 597–612.
Marinkovic K, Dhond RP, Dale AM, Glessner M, Carr V, Halgren E. Spatiotemporal dynamics of modality-specific and supramodal word processing. Neuron 2003; 38: 487–97.
Martin A. The representation of object concepts in the brain. Annu Rev Psychol 2007; 58: 25–45.
Mellet E, Tzourio N, Denis M, Mazoyer B. Cortical anatomy of mental imagery of concrete nouns based on their dictionary definition. Neuroreport 1998; 9: 803–8.
Mesgarani N, Cheung C, Johnson K, Chang EF. Phonetic feature encoding in human superior temporal gyrus. Science 2014; 343: 1006–10.

Mesulam MM. From sensation to perception. Brain 1998; 121: 1013–52.
Michalareas G, Vezoli J, van Pelt S, Schoffelen JM, Kennedy H, Fries P. Alpha-Beta and Gamma rhythms subserve feedback and feedforward influences among human visual cortical areas. Neuron 2016; 89: 384–97.
Mion M, Patterson K, Acosta-Cabronero J, Pengas G, Izquierdo-Garcia D, Hong YT, et al. What the left and right anterior fusiform gyri tell us about semantic memory. Brain 2010; 133: 3256–68.
Morán MA, Mufson EJ, Mesulam MM. Neural inputs into the temporopolar cortex of the rhesus monkey. J Comp Neurol 1987; 256: 88–103.
Mukamel R, Gelbard H, Arieli A, Hasson U, Fried I, Malach R. Coupling between neuronal firing, field potentials, and FMRI in human auditory cortex. Science 2005; 309: 951–4.
Muthukumaraswamy SD. High-frequency brain activity and muscle artifacts in MEG/EEG: a review and recommendations. Front Hum Neurosci 2013; 7: 138.
Nakai Y, Jeong JW, Brown EC, Rothermel R, Kojima K, Kambara T, et al. Three- and four-dimensional mapping of speech and language in patients with epilepsy. Brain 2017; 140: 1351–70.
Nestor PJ, Fryer TD, Hodges JR. Declarative memory impairments in Alzheimer's disease and semantic dementia. Neuroimage 2006; 30: 1010–20.
Nobre AC, Allison T, McCarthy G. Word recognition in the human inferior temporal lobe. Nature 1994; 372: 260–3.
Noppeney U, Phillips J, Price C. The neural areas that control the retrieval and selection of semantics. Neuropsychologia 2004; 42: 1269–80.
Noppeney U, Price CJ. A PET study of stimulus- and task-induced semantic processing. 2002935: 927–35.
Ojemann JG, Akbudak E, Snyder AZ, McKinstry RC, Raichle ME, Conturo TE. Anatomic localization and quantitative analysis of gradient refocused echo-planar fMRI susceptibility artifacts. Neuroimage 2002; 1997; 6: 156–67.
Oldfield RC. The assessment and analysis of handedness: the Edinburgh inventory. Neuropsychologia 1971; 9: 97–113.
Orban GA. Higher order visual processing in macaque extrastriate cortex. Physiol Rev 2008; 88: 59–89.
Otsubo H, Ochi A, Imai K, Akiyama T, Fujimoto A, Go C, et al. High-frequency oscillations of ictal muscle activity and epileptogenic discharges on intracranial EEG in a temporal lobe epilepsy patient. Clin Neurophysiol 2008; 119: 862–8.
Patterson K, Nestor PJ, Rogers TT. Where do you know what you know? The representation of semantic knowledge in the human brain. Nat Rev Neurosci 2007; 8: 976–87.
Phan TG, Fong AC, Donnan GA, Srikanth V, Reutens DC. Digital probabilistic atlas of the border region between the middle and posterior cerebral arteries. Cerebrovasc Dis 2009; 27: 529–36.
Pieters TA, Conner CR, Tandon N. Recursive grid partitioning on a cortical surface model: an optimized technique for the localization of implanted subdural electrodes. J Neurosurg 2013; 118: 1086–97.
Poldrack RA, Wagner AD, Prull MW, Desmond JE, Glover GH, Gabrieli JD. Functional specialization for semantic and phonological processing in the left inferior prefrontal cortex. Neuroimage 1999; 10: 15–35.
Quillian MR. Semantic memory. In: Minsky M, editor. Semantic information processing. Cambridge, MA: MIT Press; 1968. pp. 227–70.
Ralph MA, Jefferies E, Patterson K, Rogers TT. The neural and computational bases of semantic cognition. Nat Rev Neurosci 2016; 18: 42–55.
Saad ZS, Reynolds RC. Suma. Neuroimage 2012; 62: 768–73.
Sharp DJ, Scott SK, Wise RJS. Retrieving meaning after temporal lobe infarction: the role of the basal language area. Ann Neurol 2004; 56: 836–46.
Snodgrass JG, Vanderwart M. A standardized set of 260 pictures: norms for name agreement, image agreement, familiarity, and visual complexity. J Exp Psychol Hum Learn Mem 1980; 6: 174–215.
Spitsyna G, Warren JE, Scott SK, Turkheimer FE, Wise RJS. Converging language streams in the human temporal lobe. J Neurosci 2006; 26: 7328–36.
Tandon N. Cortical mapping by electrical stimulation of subdural electrodes: language areas. In: Luders H, editor. Textbook of epilepsy surgery. London: McGraw Hill; 2008. pp. 1001–15.
Tandon N. Mapping of human language. In: Yoshor D, Mizrahi EM, editors. Clinical brain mapping. Columbus: McGraw Hill Education; 2012. pp. 203–18.
Thompson-Schill SL. Neuroimaging studies of semantic memory: inferring "how" from "where". Neuropsychologia 2003; 41: 280–92.
Thompson-Schill SL, D'Esposito M, Aguirre GK, Farah MJ. Role of left inferior prefrontal cortex in retrieval of semantic knowledge: a reevaluation. Proc Natl Acad Sci USA 1997; 94: 14792–7.
Tulving E. Episodic and semantic memory. Organ Mem 1972; 1: 381–403.
Ungerleider LG, Mishkin M. Two cortical visual systems. In: Ingle DJ, Goodale MA, Mansfield RJW, editors. Analysis of visual behavior. Cambridge: MIT Press; 1982. pp. 549–86.
Wada J, Rasmussen T. Intracarotid injection of sodium amytal for the lateralization of cerebral speech dominance. J Neurosurg 2007; 106: 1117–33.
Wagner AD, Paré-Blagoev EJ, Clark J, Poldrack RA. Recovering meaning. Neuron 2001; 31: 329–38.
Warrington EK. The selective impairment of semantic memory. Q J Exp Psychol 1975; 27: 635–57.
Whaley ML, Kadipasaoglu CM, Cox SJ, Tandon N. Modulation of orthographic decoding by frontal cortex. J Neurosci 2016; 36: 1173–84.
Xu J, Gannon PJ, Emmorey K, Smith JF, Braun AR. Symbolic gestures and spoken language are processed by a common neural system. Proc Natl Acad Sci USA 2009; 106: 20664–9.